Published in final edited form as:
Sci Signal. ; 7(352): ra109. doi:10.1126/scisignal.2005450.

Two-pore channels provide insight into the evolution of voltage-gated Ca^{2+} and Na^{+} channels

Taufiq Rahman[1,*], **Xinjiang Cai**[2], **G. Cristina Brailoiu**[3], **Mary E. Abood**[4], **Eugen Brailoiu**[5], and **Sandip Patel**[2,*]

[1]Department of Pharmacology, Cambridge University, Cambridge CB2 1PD, UK

[2]Department of Cell Developmental Biology, University College London, London, WC1E 6BT, UK

[3]Department of Pharmaceutical Sciences, Thomas Jefferson University School of Pharmacy, Philadelphia, Pennsylvania 19107, USA

[4]Department of Anatomy and Cell Biology, and Center for Substance Abuse Research, Temple University, Philadelphia, PA 19140, USA

[5]Department of Pharmacology and Center for Substance Abuse Research, Temple University, Philadelphia, PA 19140, USA

Abstract

Four-domain voltage-gated Ca^{2+} and Na^{+} channels (Ca_V, Na_V) underpin nervous system function and likely emerged upon intragenic duplication of a primordial two-domain precursor. To investigate if two-pore channels (TPCs) may represent an intermediate in this evolutionary transition, we performed molecular docking simulations with a homology model of TPC1, which suggested that the pore region could bind antagonists of Ca_V or Na_V. Ca_V or Na_V antagonists blocked NAADP-evoked Ca^{2+} signals in sea urchin egg preparations and in intact cells that overexpressed TPC1. By sequence analysis and inspection of the model, we predicted a noncanonical selectivity filter in animal TPCs in which the carbonyl groups of conserved asparagine residues are positioned to coordinate cations. In contrast, a distinct clade of TPCs (TPCR) in several unicellular species had ion selectivity filters with acidic residues more akin to Ca_V. TPCRs were predicted to interact strongly with Ca_V antagonists. Our data suggest that acquisition of a "blueprint" pharmacological profile and changes in ion selectivity within four-domain voltage-gated ion channels may have predated intragenic duplication of an ancient two-domain ancestor.

Introduction

The voltage-gated ion channel superfamily is critical for a plethora of cellular processes in both excitable and nonexcitable cells (1). Voltage-gated Ca^{2+} channels (Ca_Vs) drive

[*]Joint corresponding authors (mtur2@cam.ac.uk or patel.s@ucl.ac.uk).

Author contributions: TR performed the modeling and docking. XC performed the phylogenetic analysis. GCB, MEA, and EB performed the microinjection and Ca^{2+} imaging experiments. SP assisted with the alignments, performed the Ca^{2+} measurements in egg homogenates, and wrote the paper with input from TR and XC.

Data and materials availability: Models are provided in the Supplementary Materials.

neurotransmitter release at nerve terminals, thereby sustaining action potentials propagated by voltage-gated Na^+ channels (Na_Vs) (2). Mutations in the genes encoding these proteins underlie many diseases ("channelopathies"), including migraine, arrhythmias and epilepsy (3). Both Ca_V and Na_V are composed of four homologous domains (DI-DIV) that assemble in a pseudotetrameric arrangement (Fig. 1A). Each domain comprises six membrane-spanning regions (S1–S6), which form the voltage sensor (S1–S4) and pore (S5–S6) (1). Ca_V and Na_V are targeted clinically by various drugs– including antihypertensives, antiarrhythmics, anticonvulsants, and local anaesthetics– primarily through interactions with S6 (4, 5). The reentrant pore loops (p-loops) located between S5 and S6 control ion selectivity. Much is known about the structure-function relationships for these proteins, including atomic insight into prokaryotic Na_V homologs (6–9).

Two-pore channels (TPCs) are less well characterized voltage-gated ion channels (10). Similar to Ca_V and Na_V, TPCs are modular proteins that are also likely to be pseudotetrameric (11–13) but they possess a distinctive structure comprising only two homologous channel domains (Fig. 1A). Additionally, they are not present on the plasma membrane but rather on acidic intracellular organelles that function as Ca^{2+} stores (14). In plants, they localize to the vacuole and correspond to SV channels that underlie the "slow vacuolar current" in response to Ca^{2+} and voltage (15). In animals, TPCs localize to the analogous vesicles within the endosomal and lysosomal system, but their function is not entirely clear. Multiple studies suggest TPCs are the target for the Ca^{2+}-mobilizing messenger NAADP (16–18). NAADP mobilizes Ca^{2+} from acidic organelles to regulate a multitude of events in various cells, including sea urchin eggs where its Ca^{2+}-mobilizing activity was first described (19, 20). Gating of TPCs by NAADP, however, is complex and likely involves accessory proteins and co-activation by the phosphoinositide $PI(3,5)P_2$ (21–23). The pharmacology of TPCs is ill-defined and the permeability properties of TPCs vary substantially between studies with reports concluding that TPCs are nonselective (24, 25) or selective for Ca^{2+} (26), Na^+ (22), or H^+ (27).

Na_Vs are thought to have evolved from Ca_Vs (2), and their emergence can be traced to unicellular organisms that were the ancestors of fungi and animals (28, 29). Ca_V-like selectivity filters in Na_Vs from basal lineages support the Ca_V to Na_V transition (28), as do functional analyses demonstrating Ca^{2+} permeability of select Na_V homologs from *Nematostella vectensis*, a simple Eumetazoan (30). Na_Vs are also present in bacteria (31), but bacterial Na_Vs are single-domain proteins that likely acquired Na^+ selectivity independently of animal Na_Vs (32). The topological similarities between the four domains of animal Ca_V and Na_V with the single domain of voltage-gated K^+ channels, which assemble as tetramers, has led to the proposal that four-domain channels evolved following two rounds of intragenic duplication of a primordial, single-domain precursor (2). The duplicated domain organization of TPCs makes them possible descendants of the putative evolutionary two-domain intermediate (33). TPCs may, therefore, hold a key position in the evolution of the voltage-gated ion channel superfamily. Definition of their properties is thus important for reconstructing ancestry of ion channel attributes. Here, we provide evidence that the structural determinants underlying channel blockade by pharmacological antagonists and ion selectivity may have been acquired prior to intragenic duplication of primeval two-

domain channels. Key features of extant voltage-gated ion channels thus emerged early in their evolution.

Results

Phylogenetic analysis of voltage-gated ion channel domains suggests a common ancestry for TPCs, Ca_Vs, and Na_Vs

The duplicated domain organization of TPCs is consistent with the relationship of TPCs to an ancient two-domain precursor that underwent intragenic duplication to give rise to four-domain channels (2). The phylogeny of extant two-domain and four-domain channels, however, is ill-defined and difficult to establish given sequence divergence. We divided TPCs, Ca_v, and Na_v members of the voltage-gated ion channel superfamily (table S1) into their individual channel domains (S1–S6). Ancestry was then probed through an "all-domain" phylogenetic analysis using the DI – DIV segments of Na_v, and Ca_v, and the DI – DII segments of TPCs (Fig. 1B). For Ca_v and Na_v, DI grouped with DIII; whereas DII grouped with DIV, consistent with an ancestral duplication event (34). Importantly, TPC domains appear phylogenetically closer to individual domains of Ca_V and Na_V, than to each other (Fig. 1B). DI of TPCs grouped with DI and DIII of Ca_Vs and Na_Vs (green); whereas DII of TPC grouped with DII and DIV of Ca_Vs and Na_Vs (purple). Each domain of TPCs may, therefore, be related to counterparts in Ca_V and Na_V supporting a common ancestry.

Ca_V antagonists target the pore region of TPCs

Ca^{2+} and Na^+ channel antagonists are thought to bind to similar regions within the pore of their respective four-domain channels. Overlap in the molecular determinants underlying drug binding and channel regulation suggests a similar structural motif for pharmacological block (35). Because TPCs, Ca_Vs, and Na_Vs are likely descended from a common ancestor, all of these voltage-gated ion channels may contain a similar structural motif within their pore regions. To test this, we generated homology models for the pore regions (S5–S6) of TPC, Ca_V, and Na_V for molecular docking analyses. The pore regions of TPCs and the single-domain prokaryotic Na^+ channels exhibit high sequence similarity (Fig. 2A), especially within S5, S6, and the first pore-helix (PH1). Therefore, we used the crystal structure of Na_V from *Arcobacter butzleri* (PDB: 3RVY) (6) as a template for homology modeling. In the structural model, TPC adopted the characteristic pyramidal structure in which four inner helices (S6) cross to form a closed bundle near the cytosolic entrance (Fig. 2B).

To test whether TPCs could bind Ca_V blockers, we performed molecular docking studies with dihydropyridines, antagonists of L-type Ca_V (Fig. 3A, Table 1). We successfully docked a series of dihydropyridines to the pore region of TPC (Fig. 3A). Analogs were tightly clustered and centrally placed in the inner cavity. The predicted free energy (ΔG) values were −4.5 to −6.5 kcal/mol (Table 1). We also docked the dihydropyridines onto models of Ca_V and Na_V and calculated ΔG values for each antagonist (Table 1) As expected, dihydropyridines docked to Ca_V with in a tight cluster biased towards the DIII–DIV interface (Fig. 3B). Although dihydropyridines docked to Na_V, the poses were less clustered than for TPC or Ca_V, segregating into either the inner cavity or the DII–DIII

interface of Na_V (Fig. 3C). This lack of consensus was most apparent from an overlay of the volume occupied by the analogs in the three channel types (Fig. 3D). The ΔG values were generally higher (less negative) for Na_V (−3.1 to −6 kcal/mol) than TPC and Ca_V (Fig. 3D, Table 1) predicting a rank order of potency for dihydropyridines of Ca_V > TPC > Na_V (Fig. 3D). Additionally, verapamil (a phenylyalkamine class of L-type Ca_V antagonist) and diltiazem (a benzothiazepine class of Ca_V antagonist) also docked to TPC (Fig. 3E, Table 1). Thus, the molecular docking simulations suggested that TPCs can bind Ca_V antagonists.

Multiple studies, although not all, indicate that TPCs are activated by NAADP (16, 17, 22, 23). Several Ca_V antagonists block NAADP-evoked Ca^{2+} signals in sea urchin egg homogenates (36) and TPC-dependent Na^+ currents in cells overexpressing TPC (22, 37). Using the sea urchin egg homogenate preparation, we showed that nifedipine, isradipine, verapamil, and diltiazem all inhibited NAADP-induced Ca^{2+} release (Fig. 3F). Thus, the molecular docking simulations and the NAADP-stimulated, Ca^{2+}-release assay suggest that Ca_V antagonists target and block the TPC pore.

Na_V antagonists target the pore region of TPCs

To test whether TPCs are targeted by Na_V antagonists, we performed a similar analysis using a series of 10 drugs, typified by the local anaesthetic lidocaine. As with the Ca_v antagonists, the Na_V antagonists docked in a tight cluster within the TPC pore (Fig. 4A) and bound with ΔG values that were similar to those calculated for these antagonists with the Na_V model (Table 2, fig. S1). Lidocaine blocked NAADP-evoked Ca^{2+} signals in the sea urchin egg homogenate preparation but had little effect on Ca^{2+} released in response to cyclic ADP-ribose (Fig. 4B), which is mediated by ryanodine receptors (38). This was expected because, although ryanodine receptors are also intracellular channels that are permeable to Ca^{2+}, they are structurally distinct from TPCs (38). Indeed, molecular docking indicated that ryanodine interacted weakly with the TPC pore (ΔG = −3.03 kcal/mol). Bupivacaine, a local anaesthetic and anti-arrhythmic agent, also selectively inhibited NAADP responses (Fig. 4B–C). The effects of lidocaine and bupivacaine on NAADP responses were concentration-dependent with half-maximal inhibitory concentrations (IC_{50}) of 1.1 ± 0.2 and 0.1 ± 0.02 mM (n=3), respectively (Fig. 4C).

Ca_V and Na_V antagonists target the pore region of TPCs through common sites

Although Ca_V and Na_V antagonists docked at similar positions within the TPC pore (Fig. 3–4), the poses obtained differed from those in models of their cognate four-domain channels, thereby ruling out template bias during model building. For example, nicardipine, which the simulations indicated interacted strongly with both TPC (ΔG = −6.5 kcal/mol) and Ca_V, (ΔG = −7.6 kcal/mol), adopted an elongated pose approximately parallel to the axis of ion conduction in TPC and a pose perpendicular to ion conduction in Ca_v (Fig. 5A). The projection of nicardipine into the DIII–DIV interface of Ca_V is similar to previously reported docking models for dihydropyridines (39).

We observed similar disparities upon close inspection of the poses for local anesthetics docked in TPC or in Na_V. The poses for several drugs were perpendicular in TPC compared with their poses in Na_V (Fig. 5B). The poses in Na_V, exemplified by mepivacaine are

consistent with the pose reported for etidocaine docked in Na_v (40). Intriguingly, we noted congruence in poses for a range of Ca_V (nicardapine, verapamil and diltiazem) and Na_V (mepivacaine) antagonists with regard to their docked positions at the cytosolic end of the TPC pore (Fig. 5C). The identified interacting residues in TPC for these antagonists mapped to S6 in each of the domains (Fig. 5D). We identify Leu^{315} (DI), Val^{318} (DI), and Val^{675} (DII) as potential determinants for both Ca_V and Na_V antagonist action at TPCs (Fig. 5D, arrowheads). Leu^{315} in DI of TPC aligns with Val^{1165} in DIII of Ca 1.2 and Ile^{1469} in DIII of $Na_V1.2$ (Fig. 5D, bold residues). These residues are amongst those identified by site-directed mutagenesis in mediating the effects of phenylalkamines in Ca_V (41) and local anaesthetics and anticonvulsants in Na_V (42) (Fig. 5B, underlined residues). These data indicated that Ca_V and Na_V antagonists likely interact at a common site in TPCs.

To test that the modeled docking data correlated with the inhibitory effects of these Ca_V and Na_V antagonists on NAADP-stimulated Ca^{2+} release, we compared predicted ΔG from the docking analyses to IC from the sea urchin egg Ca^{2+} release assays (Fig. 5E). The in silico experiments and the functional assays were positively correlated (Fig. 5E). These data support the hypothesis that TPCs are targets for both Ca_V and Na_V antagonists.

Despite the correlation between “dry” and “wet” pharmacology, some of the antagonists of Ca_Vs or Na_Vs are not entirely selective for their target four-domain channels, leaving open the possibility that our docking and functional analyses are unrelated. To bolster our hypothesis, we analyzed veratridine, which is considered a selective Na_V agonist (43). Similar to the Na_V antagonists, veratridine inhibited NAADP-, but not cyclic ADP-ribose-induced Ca^{2+} release in a concentration-dependent manner (Fig. 5F–G). This inhibition is similar to the reported inhibitory effects of the Ca_V agonist BayK 8644 on NAADP-stimulated Ca^{2+} responses (36). TPCs thus appear to possess a pharmacological site that is related to, but clearly distinct from, both Ca_V and Na_V.

Ca_V and Na_V modifiers inhibit recombinant TPC1

To further investigate the functional effects of Ca_V and Na_V antagonists on TPC activity, we characterized NAADP-evoked Ca^{2+} signals in intact SKBR3 cells expressing TPC1 (Fig. 6). Consistent with our previous analysis (44), microinjection of NAADP evoked robust Ca^{2+} signals in TPC1-expressing cells compared to mock-transfected cells (Fig. 6A). Bath exposure to nifedipine inhibited NAADP-evoked response in a concentration-dependent manner (Fig. 6B–C) with an IC_{50} (4 μM) similar to that observed for blockade of endogenous NAADP responses in sea urchin egg homogenates (27 μM, Fig. 5E). Both lidocaine and veratridine also blocked Ca^{2+} signals stimulated by NAADP in TPC1-expressing cells (Fig. 6D).

TPCs possess noncanonical selectivity filters

Ca_Vs and Na_Vs are highly selective for their respective ions, with well-defined selectivity filters comprising conserved residues in each of the four domains (typically “EEEE” in Ca_Vs and “DEKA” in Na_Vs) (1). The ion selectivity of TPCs is not clear and no structural information is available. Inspection of the model indicated that the central cavity of TPC is constricted at the luminal end by short helices in DI (residues 278–282) and DII (637–640)

corresponding to the selectivity filter of AbuNa$_V$ (Fig. 2A, yellow region). There was a notable absence of conserved charged residues in this region, consistent with studies demonstrating poor ion selectivity of TPC2 (24, 25). The alanine residue in DIV of selectivity filters in Na$_V$, however, was present in the TPC model, although the lysine of DIII, thought to be critical for Na^+ selectivity through electrostatic repulsion of Ca^{2+} (45), was not. We identified asparagine residues that were highly conserved in animal TPCs (Fig. 2A, residues highlighted in yellow), and the carbonyl groups of the side-chains projected into the pore and therefore could be appropriately positioned to coordinate cations (Fig. 7A). This arrangement is similar to the selectivity filters of Ca^{2+}-permeable glutamate receptors of the *N*-methyl-D-aspartate type (46) but differs from the selectivity filters of Ca$_V$ and Na$_V$. Indeed, the position of these putative coordinating residues is not obvious from linear sequence alignment with Ca$_V$ and Na$_V$ (Fig. 2A) (33). Thus, the modeling data suggest that TPCs possess noncanonical selectivity filters compared with the four-domain voltage-gated ion channels.

Unicellular organisms have a distinct clade of TPCs

The modeling data indicated that selectivity filters of TPCs are divergent from Ca$_V$ and Na$_V$. When did these structural changes occur? To gain insight into the evolution of ion selectivity, we inspected the genomes of unicellular organisms that hold key positions in animal evolution for TPC homologs (Fig. 7B, table S2). TPCs are present in the choanoflagellates *Monosiga brevicollis* and *Salpingoeca rosetta*, which represent close unicellular relatives of animals (47). TPCs are also present in *Capsaspora owczarzaki*, a holozoan, and *Thecamonas trahens*, an apusozoan protist, both of which are more distantly related to animals. *Thecamonas trahens* belongs to the putative unicellular sister group to Opisthokonta (animals, fungi, and related protists) (48). Three of these unicellular species possess multiple genes encoding TPCs (Fig. 7B). We used TPC sequences from these species together with those from human and sea urchin to perform a phylogenetic classification (Fig. 7C). We identified homologs of the three-member TPC family characteristic of deuterostome animals (44). However, the remaining isoforms grouped as a previously unreported clade, which we term TPCR (for TPC-related; Fig. 7C).

The selectivity filters of TPCRs are distinct

Unicellular TPC1-3 homologs possessed putative selectivity filters similar to the asparagine-lined filters predicted for animal TPCs (Fig. 7C). The residues that were predicted to function as the selectivity filters of TPCR were divergent. For example, in DI, the putative coordinating asparagine residue was conserved but the preceding residue was acidic and aligned with the coordinating acidic residues in Ca$_V$ (Fig. 7C). The presence of acidic or polar serine residues was also noted in DII (Fig. 7C). The identification of such residues in the putative selectivity filter of TPCRs suggested similarities with Ca$_V$s. Together, these analyses indicate that multiplication of the *TPC* gene may have occurred before the animal-fungal split and was followed by changes in ion selectivity within a select TPC cohort corresponding to the ancestors of Ca$_V$ and Na$_V$. Acquisition of ion selection thus may have occurred prior to the intragenic duplication event that gave rise to four-domain channels.

TPCRs interact strongly with Ca_V antagonists

Because the putative selectivity filter of the TPCR family appeared more similar to the Ca_Vs, we generated homology models for select members of TPCR and TPC from *Salpingoeca rosetta* (for which sequences of the pore appear complete) and compared docking of dihydropyridines. The molecular docking simulations showed that all but one of the dihydropyridines docked in a tight cluster at a domain interface in TPCR (Fig. 7D), which is similar to the interaction of dihydropyridines with the DIII/DIV interface in animal Ca_V (Fig. 3B). In contrast, dihydropyridines poses in the unicellular TPC models were less clustered and more central (Fig. 7D), thus resembling data from animal TPC (Fig. 3A). Importantly, the predicted ΔG values indicated that the interaction of dihydropyridines was stronger for TPCR than for TPC Table 3). These data provide further support that TPCR are similar to Ca_Vs.

Discussion

Here, we identified a putative common binding site within TPCs for Ca_V and Na_V antagonists together with a relatively “loose” pharmacological profile. These data suggested that that this motif was acquired prior to the domain duplication event(s) that led to four-domain channels. The concentration range over which TPCs were blocked by Na_V antagonists is similar to that for blockade of Na_V (49). This raises the possibility that off-target effects of Na_V antagonists on TPCs may contribute to their efficacy.

We propose that this pharmacological site underwent diversification, accounting for the relatively selective actions of Ca_V and Na_V modifiers in the four-domain lineage. Evolution of this site is unlikely to be driven directly by selection pressure at the pharmacological level, although the existence of endogenous modifiers that manipulate ion channel activity cannot be ruled out. Perhaps more likely is that emergence and subsequent divergence of the site is a secondary consequence of the selection pressures associated with an evolving pore – a key functional domain.

Our analyses also identified a novel clade of TPCs that show similarities to Ca_V with respect to both putative pharmacology and ion selection. These data suggested that acidification of selectivity filters, likely reflecting acquisition of ion selectivity again may have occurred prior to the putative domain duplication event(s) that led to four-domain channels. Molecular cloning and functional characterization of these TPCs is urgently required.

Together, our analyses predict a potential trajectory for the evolution of voltage-gated ion channels and provide a framework for probing evolutionary relevant structural attributes of these ancient ion channels.

Materials and Methods

Sequence and phylogenetic analyses

Multiple sequence alignment and phylogenetic reconstruction were performed essentially as described (28, 29). Briefly, nonredundant protein sequences were aligned using either MAFFT or T-Coffee and columns containing more than 50% gaps were subsequently

removed from the sequence alignment using GapStreeze (Gap Strip/Squeeze v 2.1.0). Unambiguous sequence alignments were then converted to PHYLIP or NEXUS format. Identifiers for metazoan and unicellular TPCs are listed in table S1 and table S2, respectively. ProtTest (50) was utilized to select the best-fit evolution model and parameter estimates for the phylogenetic analyses. Maximum likelihood phylogeny was performed using the GARLI web service (51) with the LG amino acid substitution model, empirical frequency estimation, and the four-category discrete gamma model (LG + G + F) selected by ProtTest and 100 bootstrap replicates. Consensus trees were obtained using the CONSENSE program from the PHYLIP package (Version 3.69).

Homology modeling

Homology models for the pore regions (S5–S6) of *Stronglylocentrotus purpuratus* TPC1 (accession D1J6X7) (44), *Salpingoeca rosetta* TPC1a (accession EGD80440) and TPCRb (accession EGD78654), and human $Ca_V1.2$ (accession Q13936) and $Na_V1.2$ (accession Q99250) were generated in Modeller 9.11 (http://salilab.org/modeller/) using the 2.7 Å crystal structure of voltage-gated Na^+ channel from *Arcobacter butzleri* (Na_VAb, pdb 3RVY) as a template (6). Sequences of the pore regions from each of the domains were aligned against the cognate template region using ClustalW2 (http://www.ebi.ac.uk/Tools/msa/clustalw2/). The alignments used for TPCs are shown in Fig 2A and fig. S2. Alignments for Ca_V and Na_V corresponded to those reported in (40). We used the "straightforward" alignment for Ca_V, and the adjusted alignment (around pore-helix 2) for Na_V (40). The large loops between S5 and pore-helix 1 and between pore-helix 2 and S6 in Ca_V and Na_V were excluded. For each domain, 100 models were initially generated and the best model chosen based on the discrete optimized protein energy (DOPE) score implemented within Modeller (52). Loops in TPCs were modeled using Robetta (http://robetta.bakerlab.org/) (53). Domains were assembled as tetramers using the Na_VAb structure as template. A head to tail (*trans*) arrangement for TPCs was assumed (13). Pores were further refined with KoBaMIN (http://csb.stanford.edu/kobamin) (54). The overall 3D quality of the individual domains was assessed using Molprobity (http://molprobity.biochem.duke.edu/). Boundaries and the proportion of Ramachandran-favored residues for each domain are listed in table S3.

Docking

Docking of ligands was carried out as described previously (55). Briefly, Ca_V and Na_V antagonists (obtained from the ZINC database; zinc.docking.org) were docked using AutoDock 4.2 (http://autodock.scripps.edu/). We adopted a blind docking approach using a Grid map of 80×66×84 points in 0.375 Å spacings that encompassed the entire pore cavity. Polar hydrogens and the Gasteiger partial atomic charges were added to the protein and ligands using AutoDockTools™ (http://autodock.scripps.edu/resources/adt). Only the top-ranked poses (those with the lowest free energy of interaction) of the drugs were considered. For detailed inspection and analyses of the docked poses, ligand interaction diagrams were derived using LigPlot+ (http://www.ebi.ac.uk/thornton-srv/software/LigPlus). All structural representations were prepared using the PyMOL Molecular Graphics System. PDB files for channel models and docked ligands are available in folders S1–S5.

Ca^{2+} measurements

Sea urchin egg homogenates were prepared and loaded with Ca^{2+} as described previously (56). Ca^{2+} release was measured by cuvette-based fluorimetry using the Ca^{2+} indicators fluo-3 or fluo-4 (3 μM, Invitrogen). SKBR3 cells were cultured as described previously (16) and transfected with TurboFectin 8 (Origene) using a 3:1 ratio of reagent:plasmid. The C-terminally GFP-tagged TPC1 construct from *Stronglylcentrotus purpuratus* was described in (44). Ca^{2+} imaging using Fura-2 and NAADP microinjection (pipette concentration 1 μM) were performed as described in (23). Fluorescence intensity (Fluo dyes) and ratio (Fura-2) values were normalized to values prior to stimulation and presented as F/F_0 or R/R_0, respectively. All agonists and drugs were from Sigma.

Supplementary Material

Refer to Web version on PubMed Central for supplementary material.

Acknowledgments

We thank Alisdair Gibb, Bethan Kilpatrick, Christopher J. Penny and Martin Stocker for useful discussion.

Funding: This work was supported by grants RG65196 and RG69132 from the Royal Society (to TR), BB/G013721/1 from the Biotechnology and Biological Sciences Research Council (to SP) and DA035926, DA023204 and P30 DA13429 from the National Institutes of Health (to MEA, EB and the Center for Substance Abuse, Temple University School of Medicine). TR is a Royal Society University Research Fellow. XC is an Honorary Senior Research Fellow at UCL.

References

1. Yu FH, Yarov-Yarovoy V, Gutman GA, Catterall WA. Pharmacol Rev. 2005; 57:387. [PubMed: 16382097]
2. Hille, B. Ionic channels of excitable membranes. 1. Sinauer Associates; Sunderland, Massachusets: 1984.
3. Ryan DP, Ptacek LJ. Neuron. 2010; 68:282. [PubMed: 20955935]
4. Savio-Galimberti E, Gollob MH, Darbar D. Front Pharmacol. 2012; 3:124. [PubMed: 22798951]
5. Cain SM, Snutch TP. Biofactors. 2011; 37:197. [PubMed: 21698699]
6. Payandeh J, Scheuer T, Zheng N, Catterall WA. Nature. 2011; 475:353. [PubMed: 21743477]
7. Zhang X, et al. Nature. 2012; 486:130. [PubMed: 22678295]
8. Payandeh J, Gamal El-Din TM, Scheuer T, Zheng N, Catterall WA. Nature. 2012; 486:135. [PubMed: 22678296]
9. McCusker EC, et al. Nat Commun. 2012; 3:1102. [PubMed: 23033078]
10. Clapham DE, Garbers DL. Pharmacol Rev. 2005; 57:451. [PubMed: 16382101]
11. Hooper R, Churamani D, Brailoiu E, Taylor CW, Patel S. J Biol Chem. 2011; 286:9141. [PubMed: 21173144]
12. Churamani D, Hooper R, Brailoiu E, Patel S. Biochem J. 2012; 441:317. [PubMed: 21992073]
13. Rietdorf K, et al. J Biol Chem. 2011; 286:37058. [PubMed: 21903581]
14. Patel S, Docampo R. Trends Cell Biol. 2010; 20:277. [PubMed: 20303271]
15. Peiter E, et al. Nature. 2005; 434:404. [PubMed: 15772667]
16. Brailoiu E, et al. J Cell Biol. 2009; 186:201. [PubMed: 19620632]
17. Calcraft PJ, et al. Nature. 2009; 459:596. [PubMed: 19387438]
18. Hooper R, Patel S. Adv Exp Med Biol. 2012; 740:325. [PubMed: 22453949]
19. Churchill GC, et al. Cell. 2002; 111:703. [PubMed: 12464181]

20. Lee HC, Aarhus R. J Biol Chem. 1995; 270:2152. [PubMed: 7836444]
21. Lin-Moshier Y, et al. J Biol Chem. 2012; 287:2296. [PubMed: 22117075]
22. Wang X, et al. Cell. 2012; 151:372. [PubMed: 23063126]
23. Jha A, Ahuja M, Patel S, Brailoiu E, Muallem S. EMBO J. 2014; 33:501. [PubMed: 24502975]
24. Rybalchenko V, et al. J Biol Chem. 2012; 287:20407. [PubMed: 22500018]
25. Pitt SJ, et al. J Biol Chem. 2010; 285:24925. [PubMed: 20547763]
26. Schieder M, Rotzer K, Bruggemann A, Biel M, Wahl-Schott CA. J Biol Chem. 2010; 285:21219. [PubMed: 20495006]
27. Pitt SJ, Lam AK, Rietdorf K, Galione A, Sitsapesan R. Sci Signal. 2014; 7:ra46. [PubMed: 24847115]
28. Liebeskind BJ, Hillis DM, Zakon HH. Proc Natl Acad Sci U S A. 2011; 108:9154. [PubMed: 21576472]
29. Cai X. J Membr Biol. 2012; 245:117. [PubMed: 22258316]
30. Gur BM, et al. Cell Rep. 2012; 2:242. [PubMed: 22854023]
31. Ren D, et al. Science. 2001; 294:2372. [PubMed: 11743207]
32. Liebeskind BJ, Hillis DM, Zakon HH. Curr Biol. 2013; 23:R948. [PubMed: 24200318]
33. Ishibashi K, Suzuki M, Imai M. Biochem Biophys Res Commun. 2000; 270:370. [PubMed: 10753632]
34. Strong M, Chandy KG, Gutman GA. Mol Biol Evol. 1993; 10:221. [PubMed: 7680747]
35. Hockerman GH, Peterson BZ, Johnson BD, Catterall WA. Annu Rev Pharmacol Toxicol. 1997; 37:361. [PubMed: 9131258]
36. Genazzani AA, Empson RM, Galione A. J Biol Chem. 1996; 271:11599–11602. [PubMed: 8662773]
37. Cang C, Bekele B, Ren D. Nat Chem Biol. 2014; 10:463. [PubMed: 24776928]
38. Lee HC. J Biol Chem. 2012; 287:31633. [PubMed: 22822066]
39. Tikhonov DB, Zhorov BS. J Biol Chem. 2009; 284:19006. [PubMed: 19416978]
40. Tikhonov DB, Zhorov BS. Mol Pharmacol. 2012; 82:97. [PubMed: 22505150]
41. Hockerman GH, Johnson BD, Abbott MR, Scheuer T, Catterall WA. J Biol Chem. 1997; 272:18759. [PubMed: 9228049]
42. Yarov-Yarovoy V, et al. J Biol Chem. 2001; 276:20. [PubMed: 11024055]
43. Catterall WA. J Biol Chem. 1975; 250:4053. [PubMed: 1168643]
44. Brailoiu E, et al. J Biol Chem. 2010; 285:2897. [PubMed: 19940116]
45. Heinemann SH, Terlau H, Stuhmer W, Imoto K, Numa S. Nature. 1992; 356:441. [PubMed: 1313551]
46. Burnashev N, et al. Science. 1992; 257:1415. [PubMed: 1382314]
47. King N. Curr Biol. 2005; 15:R113. [PubMed: 15723775]
48. Cavalier-Smith T, Chao EE. Protist. 2010; 161:549. [PubMed: 20537943]
49. Catterall WA, Striessnig J. Trends Pharmacol Sci. 1992; 13:256. [PubMed: 1321525]
50. Darriba D, Taboada GL, Doallo R, Posada D. Bioinformatics. 2011; 27:1164. [PubMed: 21335321]
51. Bazinet AL, Zwickl DJ, Cummings MP. Syst Biol. 2014; 63:812. [PubMed: 24789072]
52. Eswar N, et al. Curr Protoc Protein Sci. 2007; Chapter 2 Unit.
53. Kim DE, Chivian D, Baker D. Nucleic Acids Res. 2004; 32:W526. [PubMed: 15215442]
54. Rodrigues JP, Levitt M, Chopra G. Nucleic Acids Res. 2012; 40:W323. [PubMed: 22564897]
55. O'Reilly AO, et al. PLoS ONE. 2012; 7:e41667. [PubMed: 22848561]
56. Dickinson GD, Patel S. Biochem J. 2003; 375:805. [PubMed: 12914540]

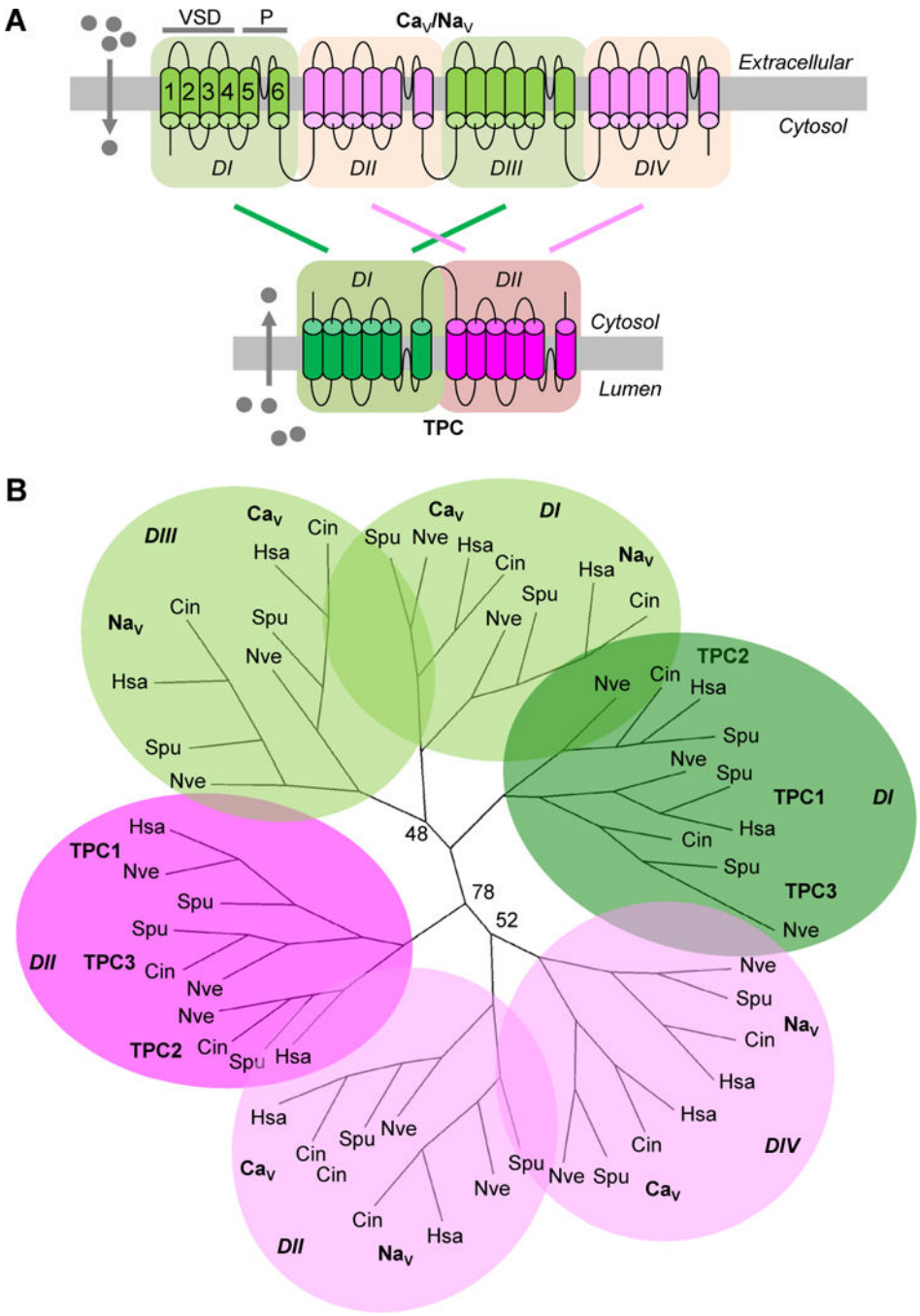

Fig. 1. Domain phylogeny of multidomain, voltage-gated ion channels

A, Schematic showing architecture of four-domain Ca_Vs and Na_Vs (top) and two-domain TPCs (bottom). Each domain (DI-DIV) comprises six transmembrane regions (S1–S6, numbered). S1–S4 form the voltage-sensing domain (VSD) and S5–S6 form the pore (P). Arrows depict the direction of ion flow into the cytosol from either the extracellular space (Ca_V and Na_V) or from the lumen of acidic organelles (TPC). **B**, Unrooted maximum likelihood tree constructed using sequences of individual domains of TPCs, Ca_Vs, and Na_Vs from representative members of the chordate, cephalachordate, echinoderm, and cnidarian

phyla. Species used were *Homo sapiens* (Hsa), the sea squirt *Ciona intestinalis* (Cin), the sea urchin *Strongylocentrotus purpuratus* (Spu), and the starlet sea anemone *Nematostella vectensis* (Nve). Accession numbers are listed in Table S1. Bootstrap values at the basal branches are shown. All other values were 40–100. Similar domains inferred from the phylogenetic relationships are shaded green (I and III) and pink (II and IV) in **B**, and connected by the colored lines in **A**.

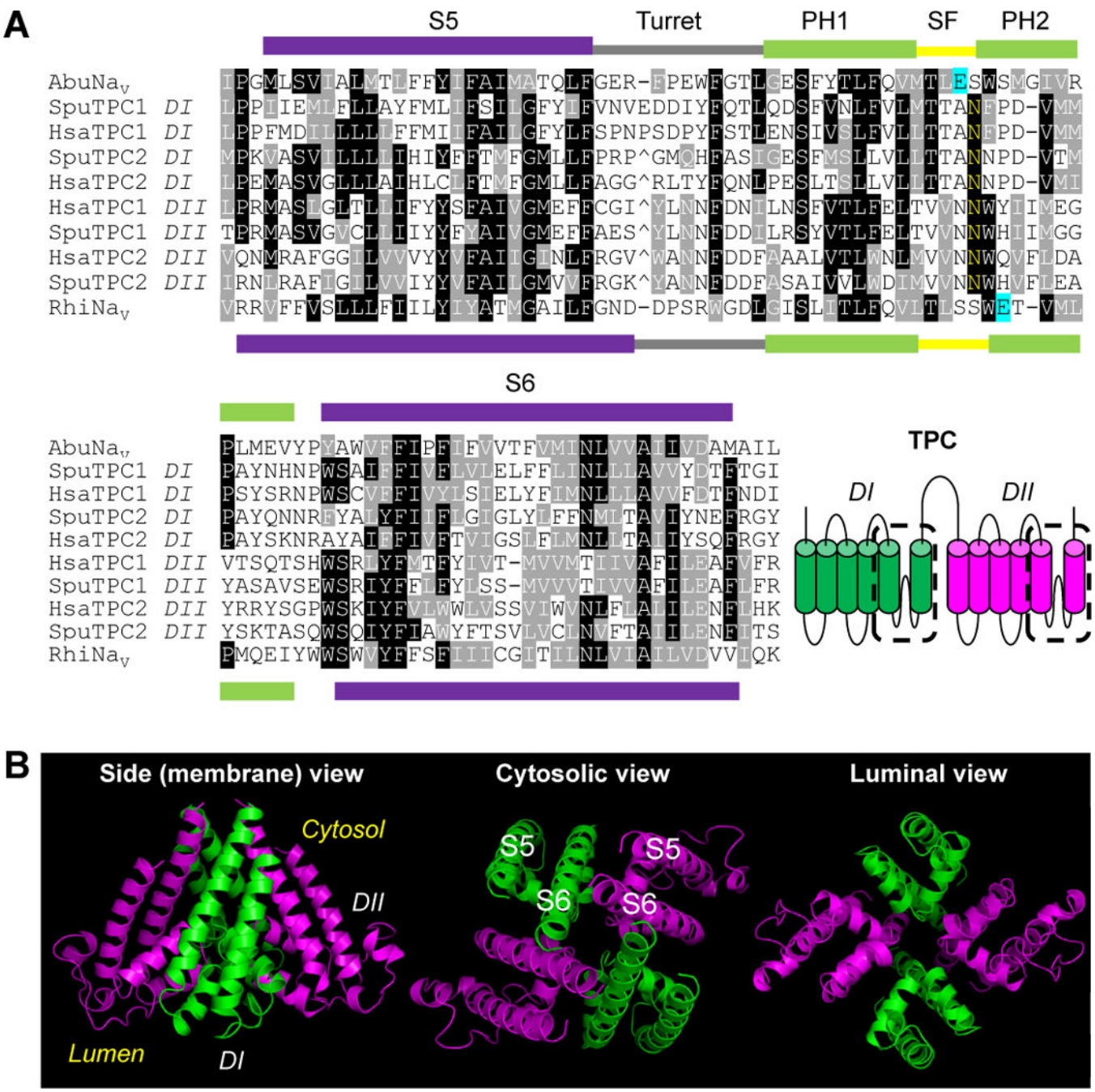

Fig. 2. A structural model of the TPC pore

A, Structure-based alignment of the pore regions of human (Hsa) and sea urchin (Spu) TPCs (outlined with dashes in schematic) with prokaryotic Na_Vs from *Arcobacter butzleri* (Abu) and *Rickettsiales sp. HIMB114* (Rhi). Positions of S5 and S6 in Na_Vs are indicated with the purple bars, the intervening turret region with a grey bar, the first (PH1) and second (PH2) pore helices with green bars, and the selectivity filter (SF) with a yellow bar. Large insertions within the corresponding turret regions of TPCs (^) were omitted from the alignment for clarity. Residues that coordinate cations in Na_V are shaded cyan. Conserved asparagine residues in TPCs within the selectivity filter are yellow. Black shading indicates

sequence identity and gray indicates conserved substitution. **B**, Homology model of the pore of sea urchin TPC1 in side (left), cytosolic (middle), and luminal (right) orientations. Side views are depicted in an upright (as opposed to inverted) “tepee” fashion to reflect their organellar (as opposed to plasma membrane) subcellular localization.

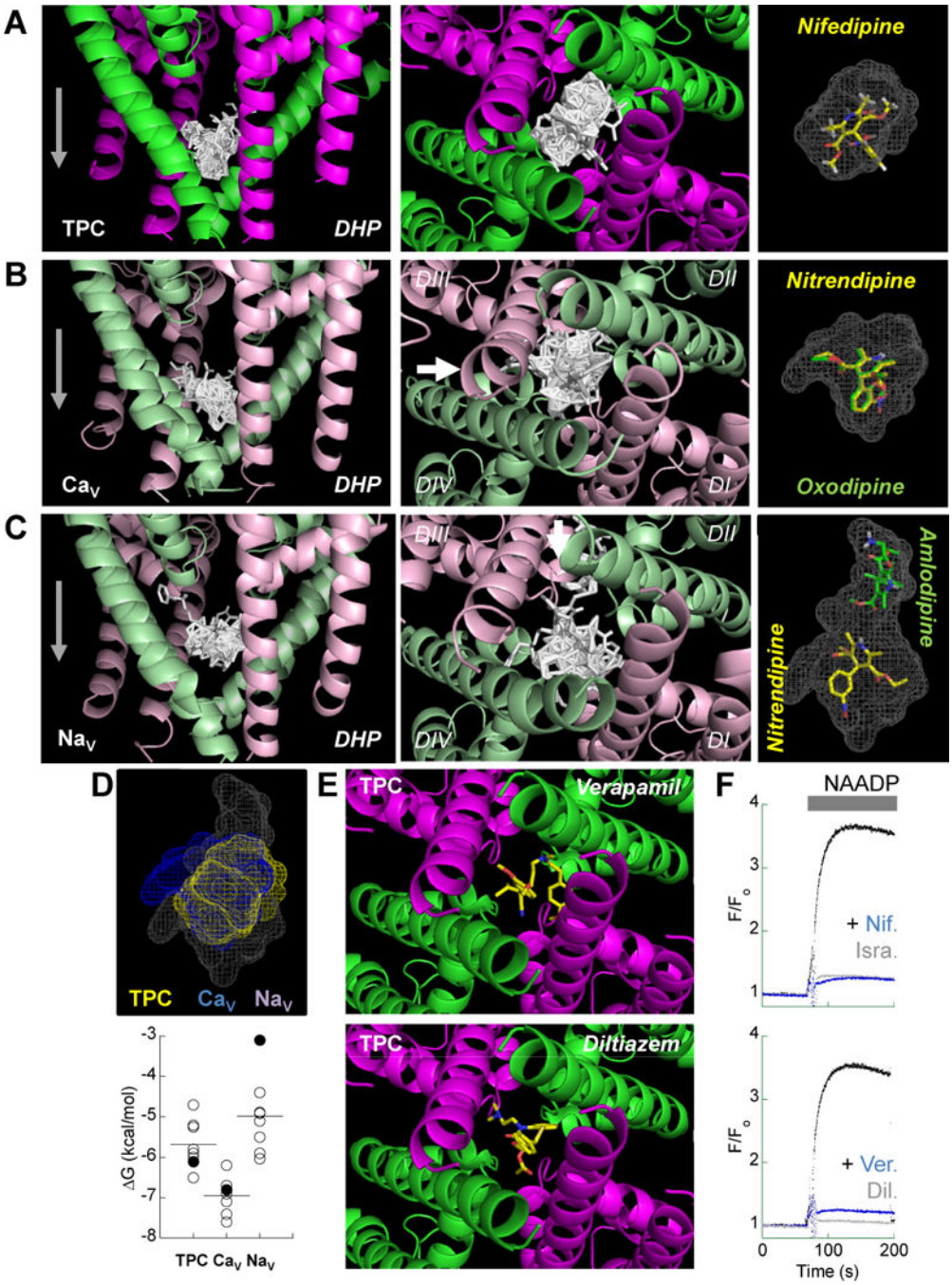

Fig. 3. Interaction of Ca_V antagonists with TPC

(A–C) Docking of a series of 8 dihydropyridines (DHP) to the pore of TPC (**A**), Ca_V (**B**), and Na_V (**C**) depicted in either side (left) or cytosolic (middle) orientations. Gray arrows depict the direction of ion flow. Right panel shows poses for all ligands represented by the gray mesh (cytosolic view) with the indicated select ligands highlighted in yellow or green. White arrows mark the interfaces between DIII–DIV (in Ca_v) and DII–DIII (Na_v). **D**, Overlay (upper panel) of dihydropyridine poses in mesh representation for TPC, Ca_V, and Na_V. Plot (lower panel) shows ΔG values for docking of ligands to the three channel types.

The closed symbols are values for nifedipine. (**E**). Docking of verapamil and diltiazem to the TPC pore (**F**). Ca^{2+} signals recorded from sea urchin egg homogenates stimulated with 1 μM NAADP in the absence (black traces) or presence (colored traces) of 100 μM nifedipine (Nif.), isradipine (Isra.), verapamil (Vera.), or diltiazem (Dil.). Data are representative of 3 experiments.

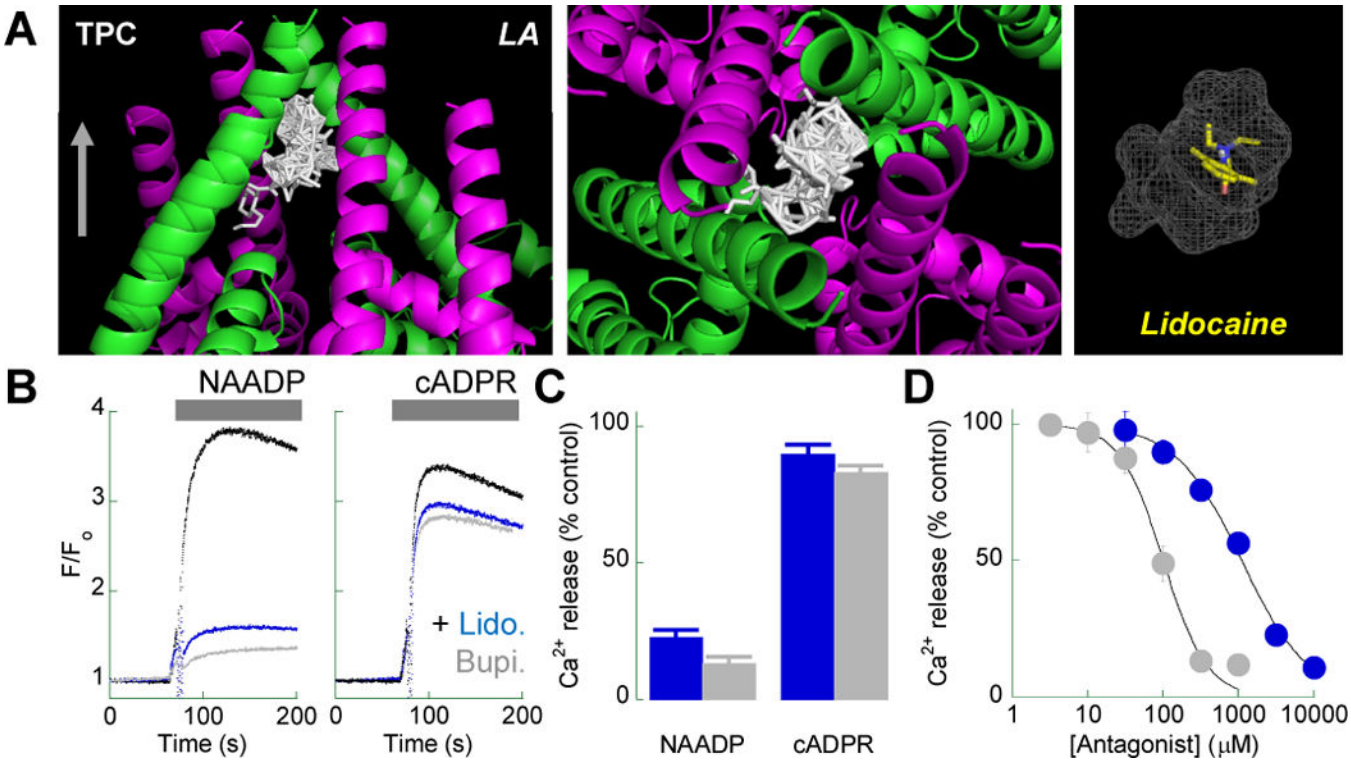

Fig. 4. Interaction of Na_V antagonists with TPC

A, Docking of a series of 10 local anaesthetics (LA) to the pore of TPC depicted in either side (left) or cytosolic (middle) orientation. Arrow depicts the direction of ion flow. Right panel shows poses for all ligands represented by the grey mesh (cytosolic view), with lidocaine highlighted in yellow. **B**, Representative Ca^{2+} signals recorded from sea urchin egg homogenates stimulated with 1 μM NAADP or 5 μM cyclic ADP-ribose in the absence (black traces) or presence of 3 mM lidocaine (blue traces) or 1 mM bupivacaine (gray traces). **C,** Pooled data (mean ± s.e.m. of 3 independent experiments) quantifying the effect of Na_V antagonists on NAADP- and cADPR-induced Ca^{2+} release. **D,** Inhibition curve showing concentration-dependent block of NAADP responses by lidocaine (blue) and bupivacaine (gray).

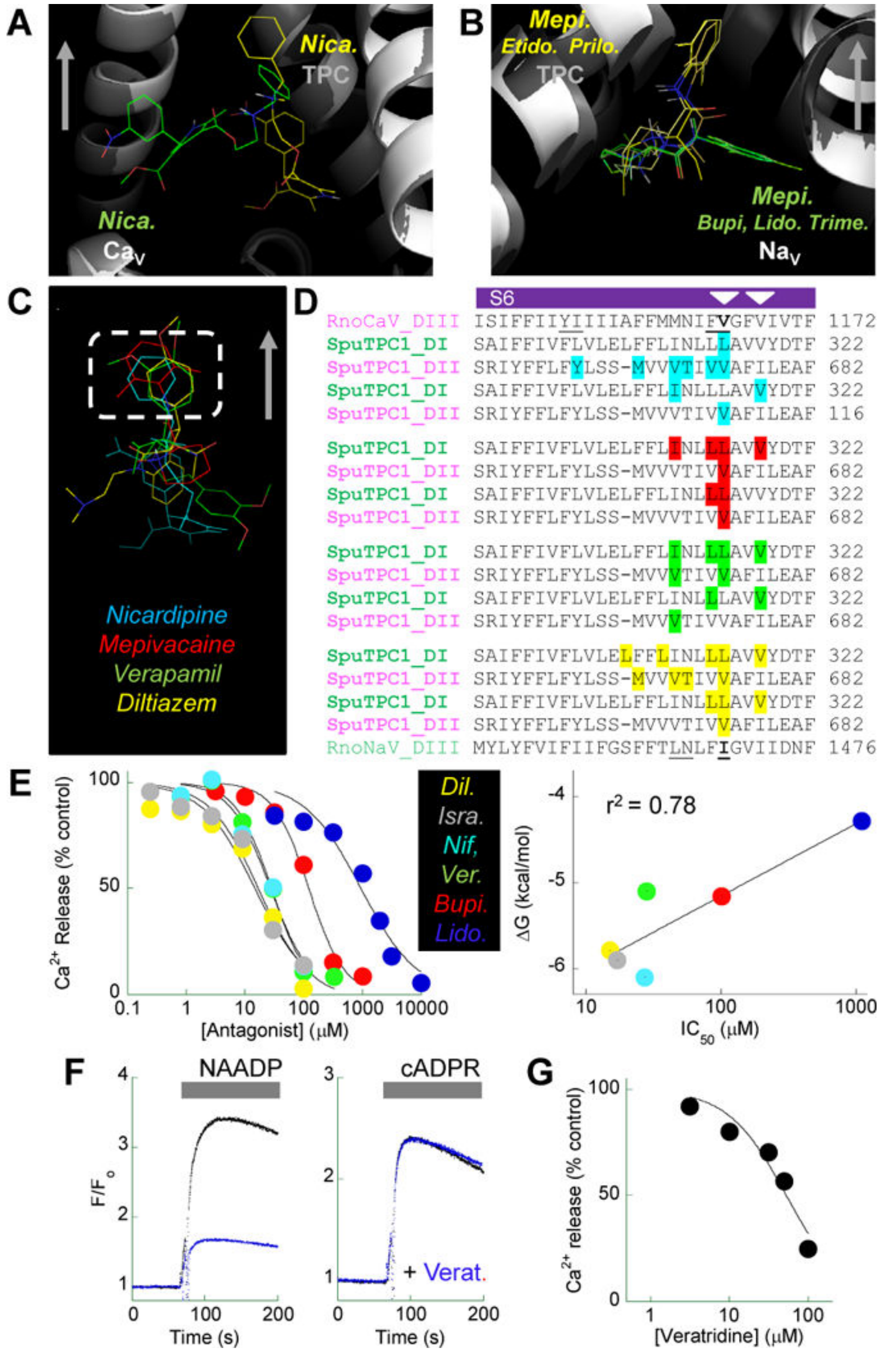

Fig. 5. Comparison of Ca_V and Na_V antagonist docking

A–B, Zoomed views comparing docking of Ca_V (**A**) and Na_V (**B**) antagonists to TPC (grey ribbons) and their cognate four domain channels (white ribbons). Ligands are colored yellow for docking to TPCs and green for docking to Ca_V and Na_V. Arrows depict the direction of ion flow. Nica., nicardipine; Mepi., mepivacaine; Etido., etidocaine; Prilo., prilocaine; Bupi., bupivacaine; Lido., lidocaine; Trime., trimecaine. **C,** Overlay of poses for the indicated Ca_V and Na_V antagonists docked to TPC. Dashed box highlights congruent nature of poses. Arrow depicts the direction of ion flow through TPC. **D**, Interacting residues within the S6

regions of DI and DII of TPC for the ligands in **C** (same color code). Arrowheads highlight residues implicated in interaction of both Ca_V and Na_V antagonists. Known molecular determinants for interactions of phenylalkylamines with rat $Ca_V2.1$ and local anaesthetics and anticonvulsants with rat $Na_v2.1$ are underlined in the corresponding S6 sequences of DIII (RnoCa$_V$, RnoNa$_V$). **E**, Inhibition curves (left) showing concentration-dependent bock of NAADP-induced Ca^{2+} release from sea urchin egg homogenates by the indicated ligands. Plot (right) showing correlation of the half-maximal inhibitory concentrations (IC_{50}) in Ca^{2+}-release assays for Ca_V and Na_V antagonists with their predicted ΔG values for docking. **F**, Representative Ca^{2+} signals recorded from sea urchin egg homogenates stimulated with 1 μM NAADP or 5 μM cyclic ADP-ribose in the absence (black traces) or presence of 100 μM veratridine (Verat., blue traces). **G**, Inhibition curve showing concentration-dependent block of NAADP responses by veratridine (IC_{50} = 52 μM, n=2).

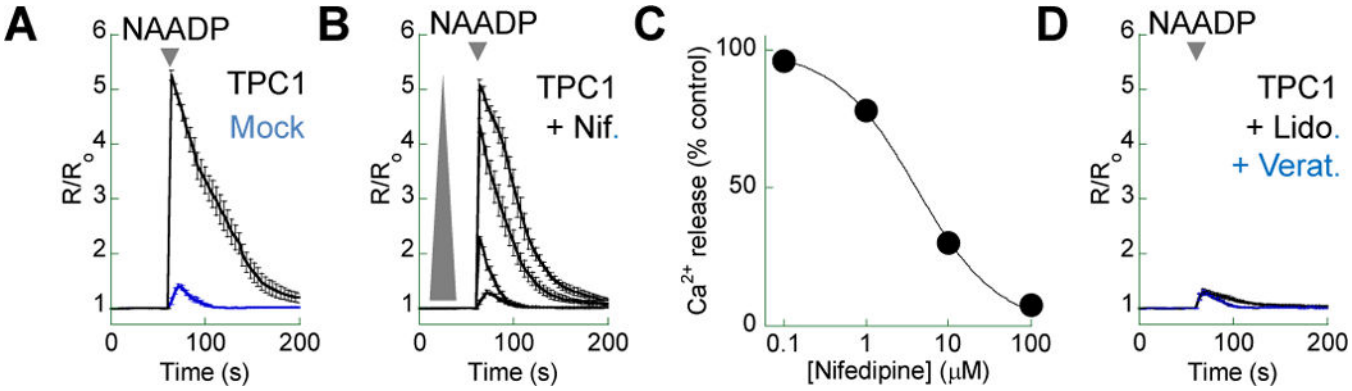

Fig. 6. Effect of Ca_V and Na_V modifiers on recombinant TPC1

Cytosolic Ca^{2+} signals from individual fura-2-loaded SKBR3 cells that were microinjected with NAADP. **A**, Responses in mock-transfected cells (blue trace) or cells transiently expressing recombinant sea urchin TPC1 (black traces). **B**, Responses in TPC1-expressing cells pre-incubated for 1 h with increasing concentrations nifedipine (Nif.). Concentrations used (from top to bottom) were 0.1, 1, 10, and 100 μM. **C**, Inhibition curve showing concentration-dependent block of NAADP responses by nifedipine. **D**, Responses in TPC1-expressing cells pre-incubated for 1 h with lidocaine (Lido. 100 μM) or veratridine (Verat. 100 μM). Results are means ± s.e.m. of 6 cells from 3 independent transfections.

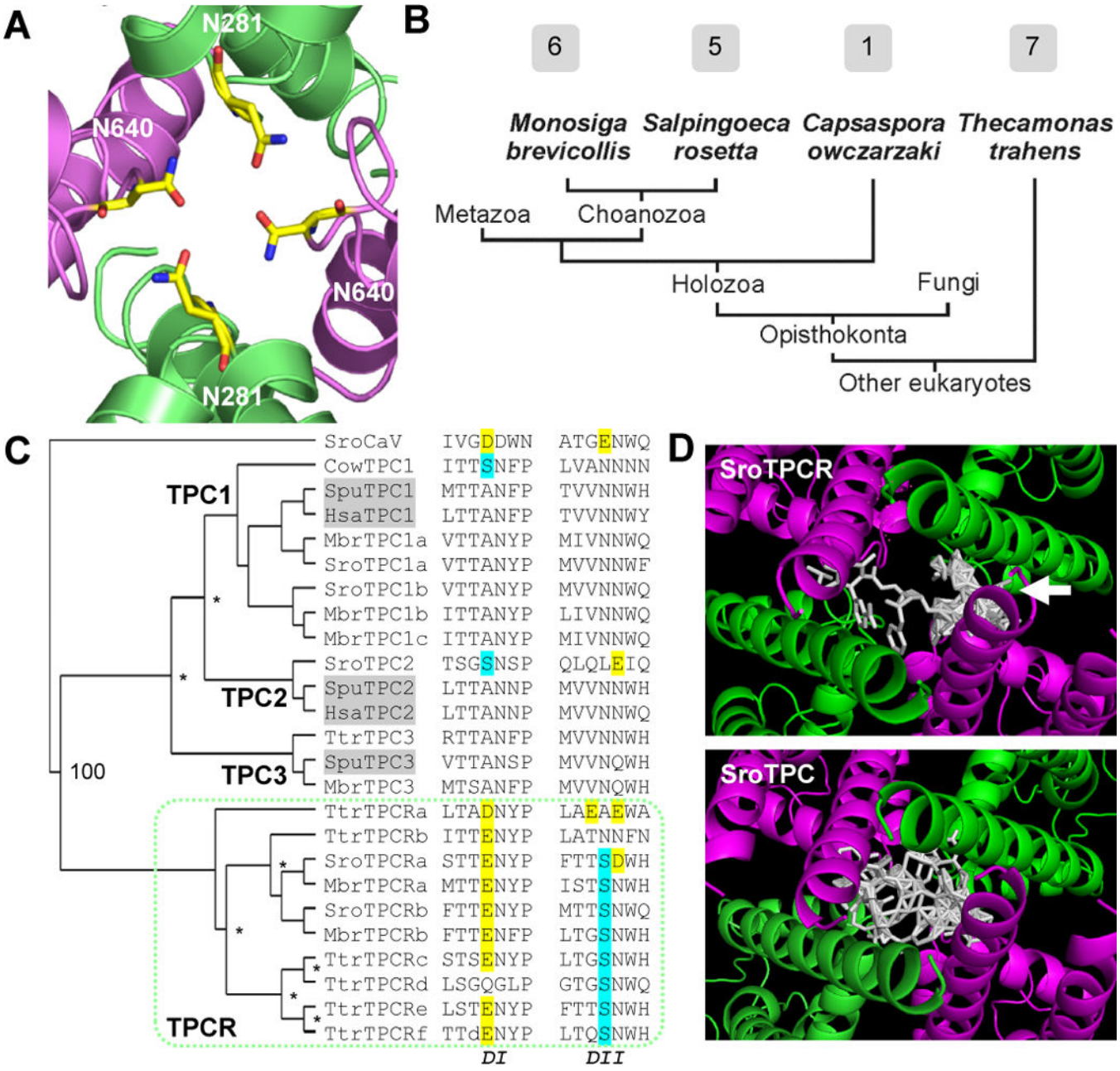

Fig. 7. Properties of TPCs from unicellular organisms

A, Zoomed view of the TPC pore showing the presence of conserved asparagine residues positioned within the putative selectivity filter to coordinate cations. **B**, Evolutionary relationships of unicellular organisms in the lineages leading to metazoans (animals). The number of identified TPCs in each of the species is shown in the boxes. **C**, Cladogram of TPC sequences of representative metazoans (Hsa, human; Spu, sea urchin; shaded), choanoflagellates (Mbr, *Monosiga brevicollis*; Sro, *Salpingoeca rosetta*), and basal species (Cow, *Capsaspora owczarzaki*; Ttr, *Thecamonas trahens*). Accession numbers are listed in table S2. Ca_V was used as the out-group (accession EGD78396.1). Bootstrap values were 81–100 except where indicated (*23–78). A previously unreported grouping (TPCR) is

highlighted by the dashed box. Sequences of the putative selectivity filters are shown to the right. Acidic (Asp, Glu; yellow) and polar (Ser; cyan) residues are shaded. **D,** Interaction of dihydropyridines with TPCR. Docking of a series of 8 dihydropyridines to the pore of TPCR (top) and TPC (bottom) from *Salpingoeca rosetta* depicted in cytosolic orientations. White arrow marks an interface between DI and DII.

Table 1

Ca_V antagonist docking to metazoan channels. ΔG values for interaction of the indicated Ca_V antagonist with TPC, Ca_V and Na_V. nd, not determined.

Ligand	ΔG TPC (kcal/mol)	ΔG Ca_V (kcal/mol)	ΔG Na_V (kcal/mol)
Amlodipine	−5.3	−6.2	−5.1
Felodipine	−5.8	−7.1	−5.5
Isradipine	−5.9	−7.4	−5.9
Nicardipine	−6.5	−7.6	−6.0
Nifedipine	−6.1	−6.8	−3.1
Nimodipine	−5.2	−6.7	−4.4
Nitrendipine	−6.0	−6.9	−4.9
Oxodipine	−4.7	−6.9	−4.9
Verapamil	−5.1	nd	nd
Diltiazem	−5.8	nd	nd

Table 2

Na_V antagonist docking to metazoan channels. ΔG values for interaction of local anaesthetics with TPC and Na_V.

Ligand	ΔG TPC (kcal/mol)	ΔG Na_V (kcal/mol)
Benzocaine	−4.9	−4.4
Bupivacaine	−5.2	−6.9
Dibucaine	−6.2	−6.3
Etidocaine	−6.0	−5.7
Lidocaine	−4.3	−5.7
Mepivacaine	−6.7	−6.8
Prilocaine	−5.8	−5.1
Procaine	−5.0	−4.9
Tetracaine	−5.1	−5.0
Trimecaine	−6.1	−6.2

Table 3

Ca_V antagonist docking to unicellular TPCs. ΔG values for interaction of dihydropyridines with TPC and TPCR from *Salpingoeca rosetta*.

Ligand	ΔG TPC (kcal/mol)	ΔG TPCR (kcal/mol)
Amlodipine	−4.9	−6.1
Felodipine	−5.0	−6.4
Isradipine	−5.3	−6.9
Nicardipine	−5.5	−7.1
Nifedipine	−5.1	−6.0
Nimodipine	−4.9	−5.1
Nitrendipine	−5.8	−5.9
Oxodipine	−5.4	−6.6